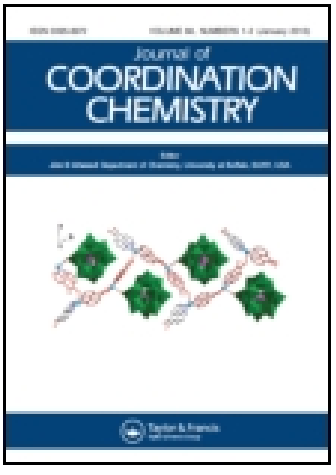

Journal of Coordination Chemistry
Publication details, including instructions for authors and subscription information:
http://www.tandfonline.com/loi/gcoo20

Synthesis, characterization, crystal structures, enzyme inhibition, DNA binding, and electrochemical studies of zinc(II) complexes

Nida Ali[a], Muhammad Nawaz Tahir[b], Saqib Ali[a], Muhammad Iqbal[a], Khurram Shahzad Munawar[a] & Sajida Perveen[c]

[a] Department of Chemistry, Quaid-I-Azam University, Islamabad, Pakistan

[b] Department of Physics, University of Sargodha, Sargodha, Pakistan

[c] Department of Soil and Environmental Sciences, Agricultural University, Peshawar, Pakistan

Accepted author version posted online: 01 Apr 2014.Published online: 23 Apr 2014.

To cite this article: Nida Ali, Muhammad Nawaz Tahir, Saqib Ali, Muhammad Iqbal, Khurram Shahzad Munawar & Sajida Perveen (2014) Synthesis, characterization, crystal structures, enzyme inhibition, DNA binding, and electrochemical studies of zinc(II) complexes, Journal of Coordination Chemistry, 67:7, 1290-1308, DOI: 10.1080/00958972.2014.910653

To link to this article: http://dx.doi.org/10.1080/00958972.2014.910653

Journal of Coordination Chemistry, 2014
Vol. 67, No. 7, 1290–1308, http://dx.doi.org/10.1080/00958972.2014.910653

Synthesis, characterization, crystal structures, enzyme inhibition, DNA binding, and electrochemical studies of zinc (II) complexes

NIDA ALI†, MUHAMMAD NAWAZ TAHIR‡, SAQIB ALI*†, MUHAMMAD IQBAL†, KHURRAM SHAHZAD MUNAWAR† and SAJIDA PERVEEN§

†Department of Chemistry, Quaid-I-Azam University, Islamabad, Pakistan
‡Department of Physics, University of Sargodha, Sargodha, Pakistan
§Department of Soil and Environmental Sciences, Agricultural University, Peshawar, Pakistan

(*Received 12 July 2013; accepted 1 February 2014*)

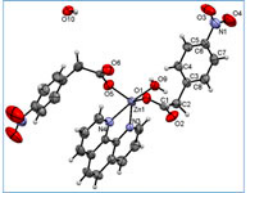

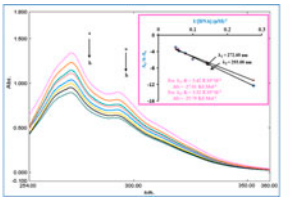

Five zinc(II) complexes, $[Zn(L^1)_2]$ (**1**), $[Zn(L^1)_2(phen)H_2O]\cdot H_2O$ (**2**), $[Zn(L^1)_2(bipy)]$ (**3**), $[Zn(L^2)_2]$ (**4**), and $[Zn(L^2)_2(phen)]$ (**5**) (where L^1 = 4-nitrophenylacetate, L^2 = phenylacetate, phen = 1,10-phenanthroline and bipy = 2,2′-bipyridine), have been synthesized and characterized by elemental analysis, FT-IR, and multinuclear NMR. Complexes **2**, **3**, and **4** have been confirmed by single-crystal X-ray diffraction. In **2** and **3**, zinc is bonded monodentate to two carboxylates exhibiting distorted trigonal bipyramidal and tetrahedral geometries, respectively, whereas in **4**, the carboxylates are bridging bidentate in distorted tetrahedral geometry. The complexes have been screened for electro- and biological activities, including DNA interaction and enzyme inhibition studies. The effect of concentration of **1–5** on the activity of enzyme, alkaline phosphatase, showed that an increase in concentration of complex decreased the activity of the enzyme. Electrochemical behavior of HL^1, **2,** and **3** was investigated by cyclic voltammetry and it was observed that ligand-centered electroactivity exhibits a proportionate change on complexation. The UV–visible spectroscopic and viscometric data indicate electrostatic and groove binding of the complexes with DNA. The binding constant and Gibb's free energy values indicate the feasibility of the complex–DNA interaction and show potent biological activity of the complexes.

Keywords: Zn(II) complexes; Crystal structures; Electrochemistry; DNA activity; Enzymatic study

1. Introduction

Metal complexes have structural diversity, remarkable physical and chemical properties, and applications as dyes, extractants, drugs, pesticides, and catalysts [1–4]. The diversity in

*Corresponding author. Email: drsa54@yahoo.com

structures of metal–organic coordination complexes comes from factors such as reaction temperature [5], counterions [6], coordination mode of metal ion [7], solvent [8], pH [9], and metal-to-ligand ratio [10]. The carboxylate ligands have variable coordination modes, such as monodentate, bidentate, tridentate, bridging, and chelating [11], and play active roles in the formation of supramolecular structure of the complexes [12].

Zinc is a fundamental component of proteins and regulates the activity of over 300 metallo-enzymes which are involved in metabolism, growth, and transfer of genetic information [13, 14]. Zinc(II) complexes are used in clinical medicine, e.g. zinc(II) acetate with erythromycin is used for the treatment of acne [15]. Synthesis and design of DNA-targeting complexes and enzyme inhibitors have significance and wide applications in chemistry, biochemistry, and medicine. These specially designed complexes convene DNA sequence selectivity and permit aromatic rings to interact with the DNA helix so as to restrict DNA replication and transcription [16, 17]. Alkaline phosphatase (ALP) is a hydrolase enzyme responsible for recycling phosphate within living cells. Zinc complexes are strong competitive inhibitors of ALP [18]. The inhibitory effect of zinc complexes has been attributed to its ability to mimic the anionic character of inorganic phosphate [19, 20]. Zinc complexes with a variety of nitrogen donors have applications in different areas of chemistry such as solution, surface and redox chemistry, luminescence, fluorescence, and organic light-emitting diodes [21–26]. 1,10-Phenanthroline and 2,2′-bipyridine are biologically important chelating ligands with planar structures, showing intra and intermolecular π–π stacking interactions, which stabilize the supramolecular structure of the resulting complexes [27].

Five Zn(II) complexes have been synthesized and characterized by spectroscopic techniques. Since zinc can effectively inhibit both ALP and phosphate transport and shows remarkable DNA interaction, the synthesized complexes have been screened for their enzymatic, DNA binding, and redox activity, and the results mutually correlated.

2. Experimental setup

2.1. *Materials*

$Zn(NO_3)_2{\cdot}6H_2O$, 4-nitrophenyl acetic acid, phenyl acetic acid, 2,2′-bipyridine, 1,10-phenanthroline, Na_2CO_3, $NaHCO_3$, and salmon sperm DNA (SSDNA) were obtained from Fluka, Switzerland. *p*-Nitrophenyl phosphate hexahydrate (*p*-NPP) was purchased from Sigma Aldrich, USA. Human serum was used as a source of ALP. Solvents were acquired from Merck, Germany, and used without drying or purification. Water used during synthesis was singly distilled.

2.2. *Physical measurements*

The melting points were determined in capillary tubes using a Gallenkamp (UK) electrothermal melting point apparatus. FT-IR spectra were recorded on a Nicolet-6700 FT-IR spectrophotometer from 4000 to 400 cm^{-1}. Elemental analysis was performed using a Leco CHNS 932 apparatus. Electrical conductivity measurements were carried out on an EC meter model Cyber Scan 500. ^1H and ^{13}C NMR spectra were recorded at room temperature on a Bruker Avance Digital 300 MHz NMR spectrometer (Switzerland) using DMSO as an internal reference [δ ^1H (DMSO) = 2.5 and δ ^{13}C (DMSO) = 40 ppm]. X-ray single-crystal

analyses were performed on a Bruker Kappa APEX-II CCD diffractometer using graphite-monochromated Mo Kα radiation ($\lambda = 0.71073$ nm). The crystal structures were solved by direct methods followed by final refinement on F^2 with full-matrix least squares using SHELXL-97 [28].

2.3. *Synthesis of 1–5*

2.3.1. [Zn(L^1)$_2$] (1). The sodium salt of HL^1 (4-nitrophenylacetic acid) was prepared by dropwise addition of methanolic solution of 4-nitrophenyl acetic acid (0.318 g, 2 mM) to an aqueous solution of sodium bicarbonate (0.168 g, 2 mM) with constant stirring at 50 °C. After neutralization, the aqueous solution of zinc(II) nitrate hexahydrate (0.297 g, 1 mM) was added dropwise. The reaction mixture was stirred for 2 h at 50 °C. The product was filtered at room temperature, washed thoroughly with distilled water, and air dried. Yield: 84%, m.p.: 259–260 °C, mol. wt.: 425. Anal. Calcd for $C_{16}H_{12}N_2O_8Zn$: C, 45.17; H, 2.80; N, 6.60. Found (%): C, 44.5; H, 2.68; N, 6.41. FT-IR (cm^{-1}): 1515 $\nu(OCO)_{asym}$, 1342 $\nu(OCO)_{sym}$, $\Delta\nu = 173$, 3082 ν(Ar–H), 2930, 1424, 709 νCH_2, 1515, 1342 $\nu(NO_2)$, 424 ν(Zn–O).

2.3.2. [Zn(L^1)$_2$(phen)·H$_2$O]·H$_2$O (2). The sodium salt of HL^1 was prepared by the same procedure as that for **1**. After 2 h stirring following the addition of zinc(II) nitrate hexahydrate (0.297 g, 1 mM), 1,10-phenanthroline (0.180 g, 1 mM) was added. Stirring was continued for another 3 h under the same reaction conditions. The final product was filtered, washed thoroughly with distilled water, and air dried. The solid was recrystallized in methanol. Yield: 82%, m.p.: 132–133 °C, mol. wt.: 641.88. Anal. Calcd for $C_{28}H_{24}N_4O_{10}Zn$: C, 52.35; H, 3.74; N, 8.72. Found (%): C, 51.61; H, 3.58; N, 8.62. FT-IR (cm^{-1}): 1582 $\nu(OCO)_{asym}$, 1345 $\nu(OCO)_{sym}$, $\Delta\nu = 237$, 3035 ν(Ar–H), 2937, 1429, 725 νCH_2, 1509, 1379 $\nu(NO_2)$, 424 ν(Zn–O), 527 ν(Zn–N).

2.3.3. [Zn(L^1)$_2$(bipy)] (3). Complex **3** was prepared and recrystallized by the same procedure as **2,** except 2,2′-bipyridine was used instead of 1,10-phenanthroline in the final step of the reaction. The final product was recrystallized in methanol. Yield: 70%, m.p.: 182–183 °C, mol. wt.: 581.83. Anal. Calcd for $C_{26}H_{20}N_4O_8Zn$: C, 53.62; H, 3.44; N, 9.62. Found (%): C, 53.41; H, 3.48; N, 9.51. FT-IR (cm^{-1}): 1598 $\nu(OCO)_{asym}$, 1344 $\nu(OCO)_{sym}$, $\Delta\nu = 254$, 3060 ν(Ar–H), 2862, 1432, 732 νCH_2, 1505, 1378 $\nu(NO_2)$, 413 ν(Zn–O), 506 ν(Zn–N).

2.3.4. [Zn(L^2)$_2$] (4). Complex **4** was obtained using the same procedure as for **1,** except phenyl acetic acid (HL^2) was used instead of HL^1. The final product was recrystallized in methanol. Yield: 82%, m.p.: 258–259 °C, mol. wt.: 335.64. Anal. Calcd for $C_{16}H_{14}O_4Zn$: C, 57.20; H, 4.17. Found (%): C, 56.97; H, 4.28. FT-IR (cm^{-1}): 1526 $\nu(OCO)_{asym}$, 1334 $\nu(OCO)_{sym}$, $\Delta\nu = 192$, 3034 ν(Ar–H), 2908, 1431, 718 νCH_2, 435 ν(Zn–O).

2.3.5. [Zn(L^2)$_2$(phen)] (5). Complex **5** was obtained using a procedure similar to that used for **2,** except HL^2 was used instead of HL^1. Yield: 78%, m.p.: 84–85 °C, mol. wt.: 515.84.

Anal. Calcd for $C_{28}H_{22}N_2O_4Zn$: C, 65.14; H, 4.26; N, 5.43. Found (%): C, 65.02; H, 4.32; N, 5.32. FT-IR (cm^{-1}): 1573 $\nu(OCO)_{asym}$, 1391 $\nu(OCO)_{sym}$, $\Delta\nu = 182$, 3059 ν(Ar–H), 2950, 1428, 723 νCH_2, 425 ν(Zn–O), 534 ν(Zn–N).

2.4. *Enzymatic activity*

Enzyme inhibition studies of zinc complexes were performed using the standard method [29], against ALP using a UV-1601 Shimadzu spectrophotometer. Working substrate was made by mixing four parts of reagent A (0.05 M Na_2CO_3–$NaHCO_3$ buffer (pH 10.0)) and one part of reagent B (*p*-nitrophenyl phosphate 50 mM dm^{-3}). Substrate was incubated for five minutes at 25 °C. In a cuvette, 2 mL of the substrate was taken and 40 µL of human serum having activity of 223 IU L^{-1} was added to it. After incubation of 1 min, absorbance was taken to confirm the activity of enzyme. ALP hydrolyzed the *p*-NPP and yellow *p*-nitrophenol was produced that absorbs at 405 nm as shown in scheme 1.

Then, various amounts of Zn complexes were added periodically from the 25 mM stock solution and again incubated for 3 min. Absorbance was recorded 1, 2, 3, 4, and 5 min thereafter. At the end, their average is taken and % inhibition was calculated.

2.5. *Cyclic voltammetry*

Voltammetric experiments were performed using an SP-300 potentiostat, serial number 0134, BioLogic Scientific Instruments, France. Measurements were carried out in aqueous DMSO (1 : 4) solution containing 0.01 M KCl, under an N_2-saturated environment in a conventional three-electrode cell with saturated silver/silver chloride (Ag/AgCl) as reference, a platinum wire as counter, and a bare glassy carbon electrode (GCE) as the working electrode. Prior to experiments, the GCE was polished with alumina (Al_2O_3) on a nylon buffing pad followed by washing with acetone and finally with distilled water. Electrochemical measurements were carried out at 25 ± 0.5 °C.

2.6. *DNA interaction study by UV–visible spectroscopy*

Commercially available SSDNA was dissolved in distilled water and kept at 4 °C for 4 days. The ratio of absorbance at 260 and 280 nm ($A_{260}/A_{280} = 1.8$–1.9) was utilized to check the purity of SSDNA (which shows that DNA is free from bound proteins) [30, 31]. The concentration of the stock solution of SSDNA, determined spectrophotometrically at 260 nm, using the molar extinction coefficient (ε) of 6600 M^{-1} cm^{-1} was 7.6×10^{-5} M [32]. Complex and solvent were taken in sample and reference cells, respectively, and spectra were

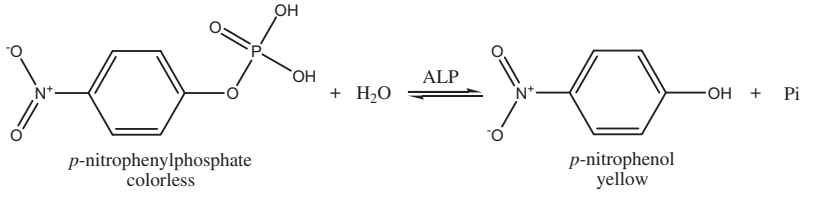

Scheme 1. Hydrolysis of *p*-NPP by ALP.

recorded using a UV-1601 Shimadzu spectrophotometer. Spectra were recorded by keeping the concentration of compound constant, while concentration of DNA was varied stepwise, using cuvettes of 1 cm pathlength at 25 ± 1 °C.

2.7. *Viscosity*

Viscosity measurements were carried out by using an Ubbelohde viscometer at 25 ± 1 °C. Flow time was determined with a digital stopwatch. Each sample was run thrice times and average flow time was calculated. Data were presented as relative viscosity, $(\eta/\eta_o)^{1/3}$, *versus* binding ratio ([complex]/[DNA]), where η and η_o are the viscosities of DNA in the presence and absence of the complex, respectively. Viscosity was calculated from the observed flow time of SSDNA containing solution (t_o), $\eta = t - t_o$ [33].

3. Results and discussion

The complexes were synthesized following the procedures described in the experimental section, dried, crystallized, and characterized through melting point, elemental analysis, FT-IR, NMR, and single-crystal XRD. The sharp melting points indicate the purity of the complexes. The elemental analyses (C, H, and N) were in agreement with the structural results obtained from single-crystal X-ray analysis.

3.1. *FT-IR data*

Carboxylate may bind monodentate or bidentate to a metal. In Zn carboxylates, it can adopt both bonding modes [34]. Carboxylate showed νOCO_{asym} bands at 1515, 1582, 1598, 1526, and 1573, while νOCO_{sym} bands at 1342, 1345, 1344, 1334, and 1391 cm^{-1} for **1–5**, respectively. The $\Delta\nu = \{\nu(OCO)_{asym} - \nu(OCO)_{sym}\}$ calculated for **2**, **3**, and **5** were 237, 254, and 182 cm^{-1}, respectively, indicating monodentate coordination of carboxylate [34]. The $\Delta\nu$ values (173 and 192 cm^{-1}) for **1** and **4** suggest bidentate bridging coordination for carboxylate. The broad bands at 3400 and 3517 cm^{-1} are attributed to OH of water in **2** and **5**, respectively. The aromatic C–H stretches were observed at 3082, 3035, 3060, 3034, and 3059 cm^{-1}, respectively, for **1–5**. The presence of nitro was confirmed by two intense bands at 1515, 1509, 1505, 1342, 1379, and 1378 cm^{-1} corresponding to the asymmetric and symmetric NOO stretches for **1–3**, respectively. In all the complexes, methylene C–H stretch was observed at 2930, 2937, 2862, 2908, and 2950 cm^{-1}, supported by the presence of bands (rocking) at 709, 725, 732, 718, and 723 and (bending) 1424, 1429, 1432, 1431, and 1428 cm^{-1}, respectively, for **1–5**. The absorptions at 413–435 cm^{-1} correspond to Zn–O vibration of **1–5**. The bands at 527, 506, and 534 cm^{-1} are attributed to Zn–N vibrations of **2**, **3**, and **5**, respectively.

3.2. *Conductivity*

The complexes are soluble in DMSO and the solutions show no electrical conductivity where $\Lambda_M < 11$ mho cm^2 M^{-1} in 10^{-3} M. Such low electrical conductance has been reported for other zinc(II) complexes in DMSO [35] as well as DMF [36].

Table 1. ^{1}H and ^{13}C NMR chemical shifts (ppm) of HL^1 and **1–3**.

	Complex			
Atom	HL^1	**1**	**2**	**3**
OH	10.36	–	–	–
H_2	3.85(s)	3.69(s)	3.52(s)	3.49(s)
H_4, H_4'	7.61(d)	7.52(d)	7.34(d)	7.60(d)
H_5, H_5'	8.19(d)	8.14(d)	8.75(d)	8.052(d)
C_1	171.2	178	175.1	175.5
C_2	39.9	42.6	43.7	43.5
C_3	142.8	140.6	140.3	140.4
C_4, C_4'	130.8	130.2	130.8	130.9
C_5, C_5'	123.2	122.8	123.2	123.3
C_6	147.0	146.6	146.6	146.5

Table 2. ^{1}H and ^{13}C NMR chemical shifts (ppm) of HL^2, **4** and **5**.

	Complex		
Atom	HL^2	**4**	**5**
OH	10.40	–	–
H_2	3.61(s)	3.44(s)	3.34(s)
H_4, H_4'	7.23–7.35(m)	7.16–7.29(m)	7.09–7.21(m)
H_5, H_5'	7.23–7.35(m)	7.16–7.29(m)	7.09–7.21(m)
C_1	174.2	177.1	179.9
C_2	40.5	43.1	43.3
C_3	134.7	137.9	136.8
C_4, C_4'	128.9	129.7	129.9
C_5, C_5'	128.1	128.4	126.7
C_6	126.5	126.3	125.1

3.3. *NMR data*

^{1}H and ^{13}C NMR chemical shifts of ligands and their complexes are presented in tables 1 and 2. A comparative NMR analysis gives evidence for complex formation and ligand coordination. The measured ^{1}H NMR spectrum of **1** revealed two signals in the aromatic region corresponding to ligand, while **2** and **3** revealed six signals in the aromatic region. Two of the latter signals were assigned to benzene of the ligand. Four peaks (at 8.94(d), 7.96–7.99 (m), 8.12(d), and 7.95(d) for **2** and 8.59(d), 7.39–7.45(m), 7.58–7.62(m), and 8.51(d) ppm for **3**) in this region were attributed to phen and bipy protons. Upon complexation, the OH peak (at 10.36 ppm) of HL^1 disappears and the upfield shift of aliphatic protons, from 3.85 to 3.69, 3.52, and 3.49 ppm for **1–3**, respectively, gives clear indication of complex formation. ^{1}H NMR spectrum of **4** revealed one signal in the aromatic region assigned to the benzene ring of the ligand. Complex **5** revealed five signals in the aromatic region, one was assigned to benzene of the ligand and the other four (at 8.99(d), 8.85–8.82(m), 8.26(d), and 8.02(d) ppm**)** were attributed to phen. OH (at 10.40 ppm) of HL^2 disappears and the upfield shift of aliphatic protons from 3.61 to 3.44 and 3.34 ppm for **4** and **5**, respectively, gives indication of complex formation. For **2** and **5,** the peak at 3.50 and 3.35 ppm gives clear indication of coordination of H_2O to zinc.

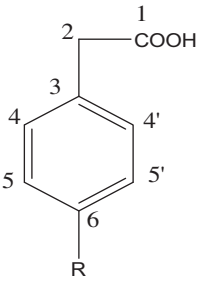

Scheme 2. Atom numbering scheme for the ligands, where R = NO_2 (**1–3**) and H (**4** and **5**).

^{13}C NMR data for HL^1 and **1–3** were also compared (table 1). In the ligand spectrum, the signal at 171.2 ppm was assigned to the carboxylate C_1. The peak position is sensitive to changes in the environment of C_1 and indicated complex formation. The acquired data showed shift of C_1 signal upon complexation to 178.1, 175.1, and 175.5 ppm for **1–3**, respectively. Another significant downfield shift upon complexation was observed for C_2 (39.9 ppm → 42.6, 43.7, and 43.5 ppm in **1–3**, respectively). These peak shifts were evidence for complexation of ligand with zinc. The peaks at 149.7, 125.8, 139.8, 128.8, 127.3, and 146.0 and 146.8, 121.9, 140.4, 123.8, and 149.3 ppm were characteristic for phen and bipy, respectively. ^{13}C NMR spectrum of HL^2 (table 2) revealed the signal at 174.23 ppm, which was assigned to carboxylate C_1. For **4** and **5**, NMR data showed shift of the C_1 signal upon complexation to 177.1 and 179.9 ppm, respectively. Another significant downfield shift upon complexation was observed for C_2 (40.5 ppm → 43.1 and 43.3 ppm for **4** and **5**, respectively). These peak shifts were evidence for complexation of the ligand. In **5**, peaks at 148.9, 125.8, 139.3, 128.8, 127.7, and 146.6 ppm were characteristic for phen. Atom numbering of the ligands is shown in scheme 2.

3.4. *Single-crystal X-ray analysis*

3.4.1. Crystal structure of 2. The molecular structure of **2** is shown in figure 1, while structure refinement parameters and selected bond lengths and angles are listed in tables 3 and 4, respectively. Zn in **2** is five-coordinate, chelated by two nitrogens of phen, two oxygens from different carboxylates, and one water (figure 1). The structural distortion index τ ($\tau = \alpha - \beta/60$, where α and β correspond to consecutive largest basal angles around Zn) was calculated as 0.684 and clearly indicated a highly distorted trigonal bipyramidal geometry. The τ-values of square-based pyramidal and trigonal-bipyramidal extremes are 0 and 1, respectively [37]. At the axial sites, oxygen of water and one nitrogen of 1,10-phenanthroline are present. The equatorial sites are occupied by the remaining nitrogen of phen and oxygens from two monodentate carboxylates. Carboxylate Zn–O distances were different from each other where the longer Zn–O distance [2.0239(16) Å] was found associated with shorter C–O [1.252(3) Å] distance and vice versa. This asymmetric mode of coordination is due to more shifting of electron density from C–O bond towards Zn in the former. The Zn–O_{water} bond distance is 2.0575(19) Å. Zn–N bond lengths of phen are asymmetrical, 2.135(2) and 2.1791(19) Å, as observed in many structurally related zinc complexes viz., $[Zn(bba)_2(phen)]$ [38], $[Zn(L)(phen)(H_2O)]_n$ [39], $[Zn(Hcit)(phen)(H_2O)]$ [40],

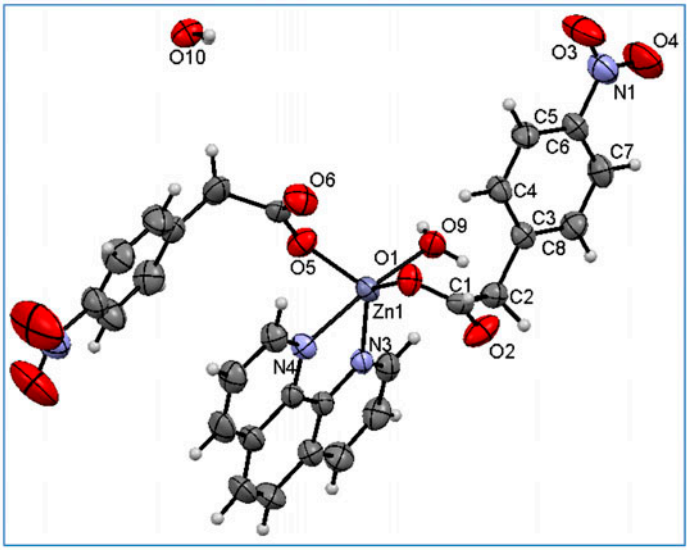

Figure 1. ORTEP diagram of **2**.

Table 3. Crystal data and structure refinement parameters for **2–4**.

Complex	**2**	**3**	**4**
Chemical formula	$C_{28}H_{24}N_4O_{10}Zn$	$C_{26}H_{20}N_4O_8Zn$	$C_{16}H_{14}O_4Zn$
Formula weight	641.88	581.83	335.64
T (K)	296(2)	296(2)	296(2)
Wavelength (Å)	0.71073	0.71073	0.71073
Crystal system	Monoclinic	Monoclinic	Monoclinic
Space group	$P2_1/n$	$C2/c$	$P2_1/c$
a (Å)	7.5830(7)	27.031(4)	30.221(4)
b (Å)	11.5103(8)	12.805(5)	4.9035(6)
c (Å)	31.440(3)	7.142(5)	9.5856(11)
α (°)	90	90	90
β (°)	95.769(3)	98.674(5)	92.430(6)
γ (°)	90	90	90
V (Å^3)	2730.2(4)	2444(2)	1419.2(3)
Z	4	4	4
Absorption coefficient (mm^{-1})	0.974	1.066	1.743
F (0 0 0)	1320	1192	688
Crystal size (mm)	0.34 × 0.22 × 0.20	0.30 × 0.16 × 0.14	0.30 × 0.20 × 0.18
θ range for data collection (°)	1.89–26.00	1.52–26.00	2.70–26.00
Reflections collected	5361	2397	2767
Independent reflections	4025	1869	2010
Goodness-of-fit on F^2	1.020	1.171	1.023
Final R indices [$I > 2\sigma(I)$]	$R_1 = 0.03655$, $wR_2 = 0.0764$	$R_1 = 0.0638$, $wR_2 = 0.1777$	$R_1 = 0.0442$, $wR_2 = 0.0939$
R indices (all data)	$R_1 = 0.057$, $wR_2 = 0.0844$	$R_1 = 0.0835$, $wR_2 = 0.1894$	$R_1 = 0.0724$, $wR_2 = 0.1023$
Data/restraints/parameters	5361/0/391	2397/0/178	2767/0/155

Table 4. Selected bond lengths and angles of **2**.

Bond length (Å)	
Zn–O(1)	2.0121(16)
Zn–O(5)	2.0239(16)
Zn–O(9)	2.0575(19)
Zn–N(3)	2.135(2)
Zn–N(4)	2.1791(19)
Bond angle (°)	
O1–Zn–O5	131.25(7)
O1–Zn–O9	92.05(7)
O1–Zn–N3	131.92(6)
O1–Zn–N4	89.86(6)
O5–Zn–O9	93.65(7)
O5–Zn–N3	95.33(7)
O5–Zn–N4	90.14(7)
O9–Zn–N3	96.70(7)
O9–Zn–N4	173.00(7)
N3–Zn–N4	77.06(7)

Table 5. Selected bond lengths and angles of **3**.

Bond length (Å)	
Zn–O(1)	1.952(4)
Zn–N(2)	2.083(4)
Bond angle (°)	
O1–Zn–O1	118.1(2)
O1–Zn–N2	117.89(15)
O1–Zn–N2	108.92(15)
N2–Zn–N2	79.3(2)
O1–Zn–C1	106.36(16)
O1–Zn–C1	28.55(16)
N2–Zn–C1	132.63(15)
N2–Zn–C1	102.51(15)
C1–Zn–C1	109.1(2)

[Zn(ida)(phen)(H_2O)] [41], [Zn(pzdc)(phen)4H_2O]$_n$ [42] (where bba = 2-benzoylbenzoato, L = 2,2′-(naphthalene-1,5-diylbis(oxy))diacetic acid, Hcit = citric acid, ida = iminodiacetic acid, pzdc = pyrazine-2,3-dicarboxylic acid and phen = 1,10-phenanthroline). The O1–Zn–O5 angle is 131.25(7)° as opposed to the ideal value of 180°, indicating that the geometry is distorted trigonal bipyramidal. The lattice waters play important roles in the development of supramolecular structures as shown in figure 2. The packing is aided by interaction of oxygen of nitro with hydrogens of phen and phenyl.

3.4.2. Crystal structure of 3. The molecular structure of **3** is shown in figure 3, while the structure refinement parameters and selected bond lengths and angles are listed in tables 3 and 5, respectively. Zn is four-coordinate, chelated by bipy and two oxygens of two monodentate carboxylates in distorted tetrahedral geometry (figure 3). The Zn–O (1.952(4) Å) and Zn–N (2.083(4) Å) bond distances are shorter than those found in [Zn(pydc)(bipy)(H_2O)]·2H_2O [43] and [Zn_2(H_2cit)$_2$bipy$_2$] [44], but are nearly equal to those found in [Zn(btdc)(bipy)]$_n$ [45] (where pydc = 2,3-pyridinedicarboxylic acid, H_2cit = citric acid and

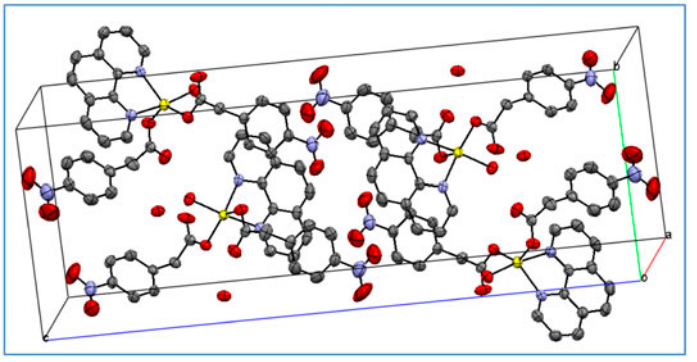

Figure 2. Packing diagram of **2**. Hydrogens have been removed for clarity.

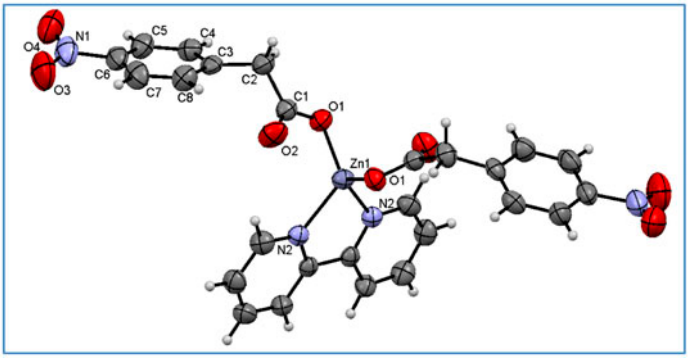

Figure 3. ORTEP diagram of **3**.

H_2btdc = 2,2′-bithiophene-5,5′-dicarboxylic acid). The O–Zn–O bond angle is 118.1(2)°, while the O–Zn–N bond angles are 108.92(15)°–117.89(15)° showing that the geometry around zinc is distorted tetrahedral.

The crystal packing is formed by a large number of intermolecular associations in which oxygen, hydrogen, and nitrogen take part. Hydrogen of bipy interacts with oxygen of nitro of the ligand at 2.683 Å, assisting the arrangement of molecules along the *a*-axis. The overall packing is assisted by interaction of oxygens of carboxylate with hydrogens of phenyl and methylene of ligand at 2.654 and 2.621 Å, respectively, as shown in figure 4.

3.4.3. Crystal structure of 4. The ORTEP of **4** is shown in figure 5, while refinement parameters and selected bond lengths and angles are collected in tables 3 and 6, respectively. The structure of **4** is polymeric where each zinc is four-coordinate to four oxygens of four different carboxylates exhibiting distorted tetrahedral geometry. All O–Zn–O angles are 101.66°–114.52°. The carboxylates coordinate Zn asymmetrically, with Zn–O bond distances for O1, O2, O3, and O4 of 1.957(2), 1.942(2), 1.951(3), and 1.968(2) Å, respectively. The C–O bond distances are also unequal; shorter Zn–O bonds are associated with longer O–C distances and vice versa. The crystal packing is formed principally by weak interactions among oxygens of carboxylate and hydrogens of methylene as shown in figure 6.

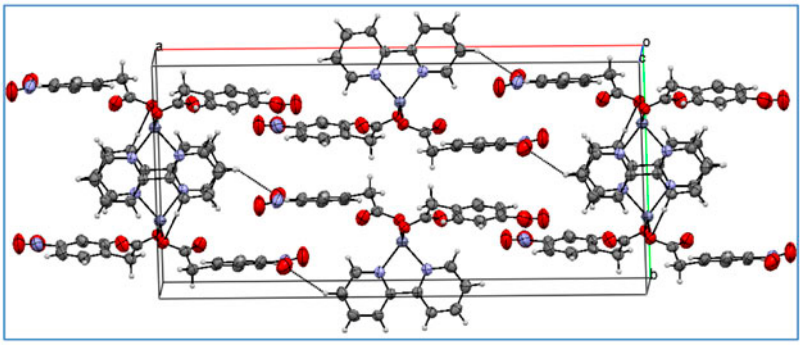

Figure 4. Supramolecular structure of **3**.

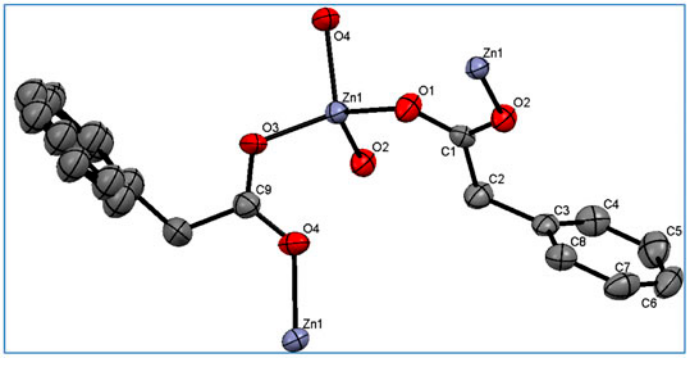

Figure 5. ORTEP diagram of **4**.

Table 6. Selected bond lengths and angles of **4**.

Bond length (Å)	
Zn–O(1)	1.957(2)
Zn–O(3)	1.951(3)
Zn–O(4)	1.968(2)
Zn–O(2)	1.942(2)
Bond angle (°)	
O1–Zn–O3	114.52(11)
O1–Zn–O4	101.66(11)
O1–Zn–O2	111.04(10)
O3–Zn–O4	107.88(11)
O2–Zn–O3	111.39(10)
O2–Zn–O4	109.81(9)

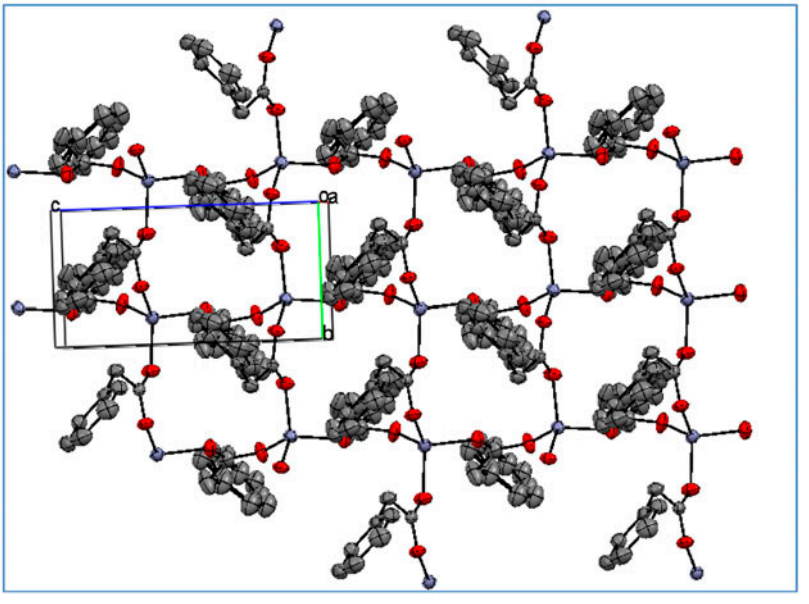

Figure 6. 2-D polymeric structure of **4** in the *abc* plane.

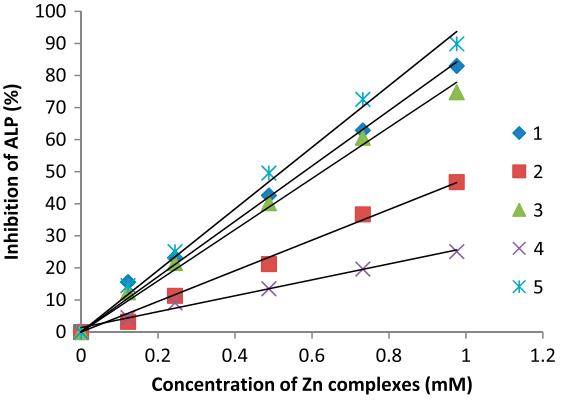

Figure 7. Inhibition profile of ALP at various concentrations of zinc complexes.

3.5. *Enzyme inhibition studies*

The influence of different concentrations of the complexes on activity of ALP was studied. ALP activity in the presence and absence of inhibitor was measured spectrophotometrically using *p*-nitrophenylphosphate as the substrate which gives yellow *p*-nitrophenol upon hydrolysis that helps to monitor the reaction. Increasing concentration of zinc complexes decreases the activity of the enzyme as shown in figure 7. This proportionate decrease in the activity of ALP with increase in the concentration of complexes indicates anti-enzymatic activity.

Surprisingly, **5** was most active among all the screened complexes. It is considered that Zn ions are released in the solution and bind to the enzyme. There is also a possibility that it may replace Mg ions present at the active site of ALP. As a result, there is less production of *p*-nitrophenol and hence decrease in absorption. **5** inhibits the enzyme up to 90% even at very low concentration, e.g. 1 mM. After this, **1** and **3** were most active against inhibition of ALP. We can assume that they have nitro attached to the benzene ring, analogous to the nitro of *p*-NPP. Hence, it may competitively bind with the enzyme and reduce the catalytic activity. Complex **4** was least active. Both ligands were inactive towards inhibition of ALP.

3.6. *Cyclic voltammetry*

Electrochemical properties of HL^1, **2,** and **3** were recorded in aqueous DMSO solution on a GCE as illustrated in figure 8. The ligand is redox active displaying two irreversible redox couples at $E_{p1/2}$ of −0.825 and −1.132 V, corresponding to the reduction of nitro to nitro radical anion and radical dianion, respectively [46, 47]. On complexation to Zn(II), the redox potential is shifted to less negative values. In **2**, the oxidation peak of the first redox couple of the ligand vanished, while the reduction peak shifted from −0.8 to −0.65 V and $E_{1/2}$ of the second redox couple is shifted from −1.132 to −0.9 V. In **3**, the first and second redox couples shift from $E_{1/2}$ values of −0.825 and −1.132 V to −0.72 and −1.0 V, respectively. This behavior of nitro containing ligands has been observed in reported Zn(II) complexes [46, 47]. The shifting of redox potential to less negative region is in accord to the electron-withdrawing influence of Zn^{2+} as a result of complexation, where carboxylate oxygens of the ligand have formal positive charge. Induction of positive charge on the ligand surface causes reduction at less negative potential. Since phen and bipy have similar binding, they have similar positive inductive property.

3.7. *UV–visible spectroscopy*

The interaction of zinc complexes with SSDNA was studied using UV–visible spectroscopy via monitoring the changes in absorption properties of complexes. The effect of varying concentration of SSDNA (100–800 µM) on absorption spectra of 2 mM solutions of **1–3**

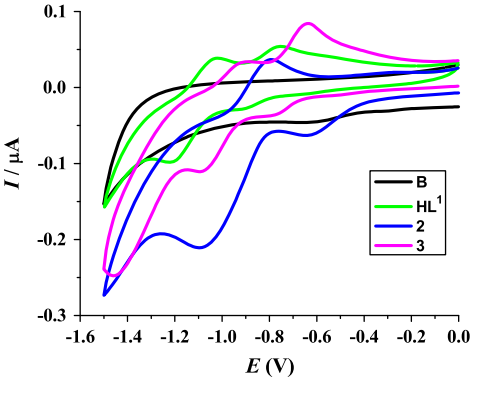

Figure 8. Cyclic voltammograms of solvent system (B), HL^1, **2** and **3**.

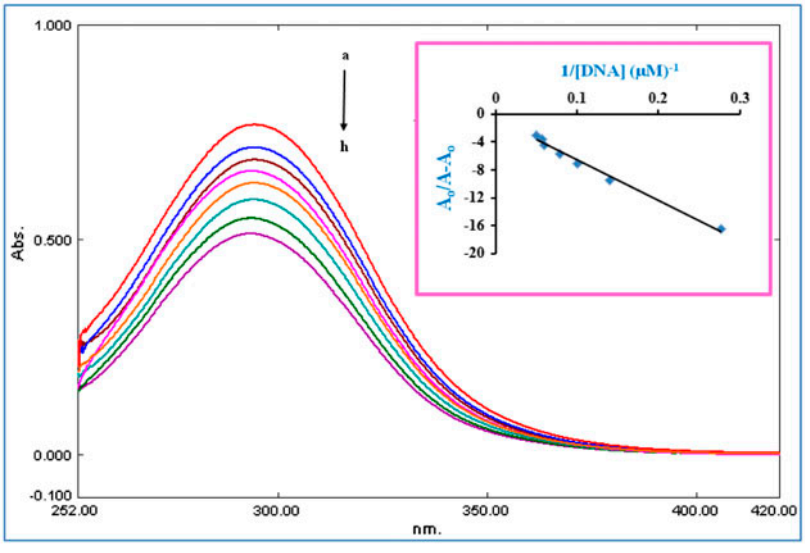

Figure 9. Absorption spectra of 2 mM **1** in the absence (a) and presence of 3.6 (b), 6.9 (c), 9.9 (d), 12.6 (e), 15.2 (f), 17.5 (g), and 17.5 (h) μM SSDNA. The arrow direction indicates increasing concentration of SSDNA.

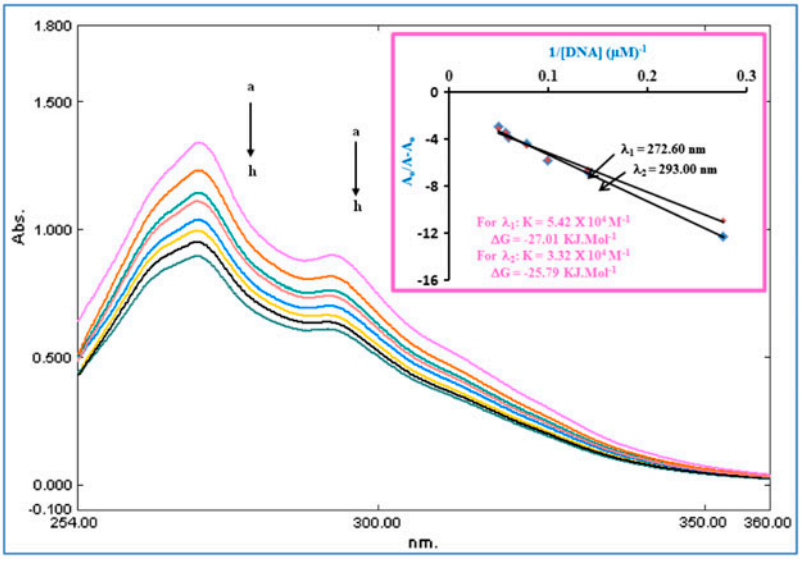

Figure 10. Absorption spectra of 2 mM **2** in the absence (a) and presence of 3.6 (b), 6.9 (c), 9.9 (d), 12.6 (e), 15.2 (f), 17.5 (g), and 17.5 (h) μM SSDNA. The arrow direction indicates increasing concentration of SSDNA.

and **5** is shown in figures 9–12. Spectra of **1** and **3** exhibited a single broad absorption at 252–330 nm, while **2** and **5** exhibited two absorptions at 254–320 and 252–310 nm. The strong absorption of these compounds in the near UV region (272–295 nm) is attributed to

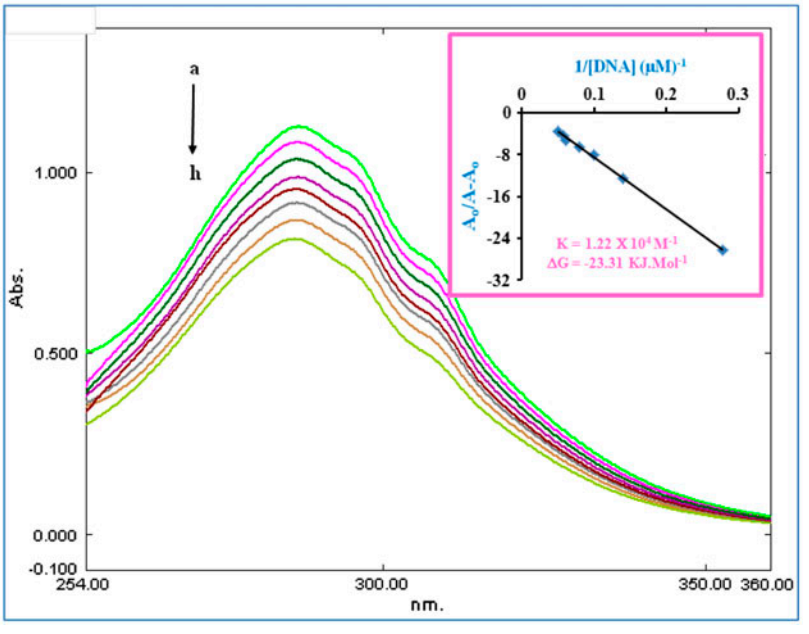

Figure 11. Absorption spectra of 2 mM **3** in the absence (a) and presence of 3.6 (b), 6.9 (c), 9.9 (d), 12.6 (e), 15.2 (f), 17.5 (g), and 17.5 (h) μM SSDNA. The arrow direction indicates increasing concentration of SSDNA.

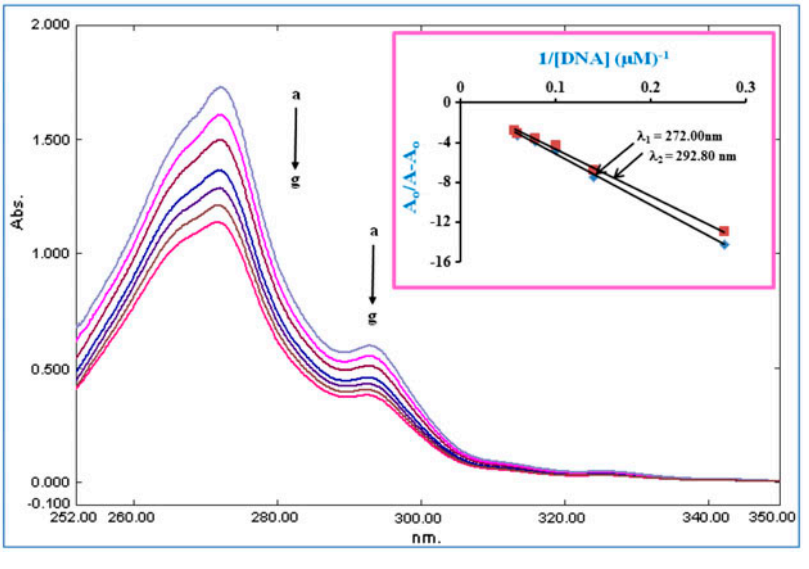

Figure 12. Absorption spectra of 2 mM **5** in the absence (a) and presence of 3.6 (b), 6.9 (c), 9.9 (d), 12.6 (e), 15.2 (f), and 17.5 (g) μM SSDNA. The arrow direction indicates increasing concentration of SSDNA.

the long-lived triplet excited state of the aromatic system [48]. The λ_{max} of the complexes exhibited slight blue shift and pronounced hypochromism by incremental addition of SSDNA. Hypochromism may be due to compactness in the structure of either the complexes alone and/or SSDNA after the formation of complex–DNA adducts [49]. The binding of **1–3** and **5** to SSDNA caused a blue shift of 1.4, 0.4, 0.8, and 0.4 nm, respectively. Such spectral characteristics are indicative of their interaction with SSDNA by mixed binding mode (electrostatic and groove binding). By using the Benesi–Hildebrand equation [50], the difference in absorbance and wavelength can be used for determination of binding parameters:

$$\frac{A_o}{A - A_o} = \frac{\varepsilon_G}{\varepsilon_{H-G} - \varepsilon_G} + \frac{\varepsilon_G}{\varepsilon_{H-G} - \varepsilon_G} \times \frac{1}{K\,[\mathrm{DNA}]} \quad (1)$$

where K is binding constant, A and A_o are absorbance of complex–DNA solution and pure complex solution, and ε_{H-G} and ε_G are the molar absorption coefficients of complex–DNA adduct and complex, respectively. The binding constant was calculated from the intercept to slope ratio of $A_o/A - A_o$ *versus* 1/[DNA] plots as shown in figures 9–12. The Gibb's free energy (G) for the process was obtained from $\Delta G = -RT\ln(K)$. The binding constant and Gibb's free energy values are listed in table 7. The negative values of Gibb's free energy in all the complexes indicate spontaneity of the complex–DNA interaction. The order found for the *Kb* values of the complexes was: **2** > **1** > **3** > **5**. The lower value of the binding constant of **5** is attributable to its bulky structure and lower diffusibility through biological membranes. The *Kb* values of **1**, **2**, and **3** are higher than [51] and comparable to [52–54], some already reported zinc complexes.

3.8. *Viscosity measurements*

The mode of interaction of the complexes with SSDNA was further explored from viscosity measurements. The viscosity of DNA is sensitive to change in DNA length; therefore, relative viscosity measurements have proved a reliable method for determining the mode of interaction of metal complexes with DNA. In case of intercalative binding mode, reversible inclusion of a molecule between DNA base pairs takes place, resulting in enlargement of the DNA helix and subsequent increase in DNA viscosity. On the other hand, groove binding and electrostatic interactions do not lengthen the DNA molecule; as a result, the DNA viscosity is decreased or remains unaffected [55]. A series of solutions were made by keeping the concentration of SSDNA constant (7.6×10^{-5} M) and varying the concentration of **1–5** and flow time was measured. A plot of $(\eta/\eta_o)^{1/3}$ *versus*

Table 7. Binding constant and Gibb's free energy values of **1–3** and **5**.

	$\lambda 1$		$\lambda 2$	
Complex	K (M^{-1})	G (kJ M^{-1})	K (M^{-1})	G (kJ M^{-1})
1	1.36×10^4	−23.55	–	–
2	5.42×10^4	−27.01	3.32×10^4	−25.79
3	1.22×10^4	−23.31	–	–
5	6.8×10^2	−16.18	2.34×10^2	−13.52

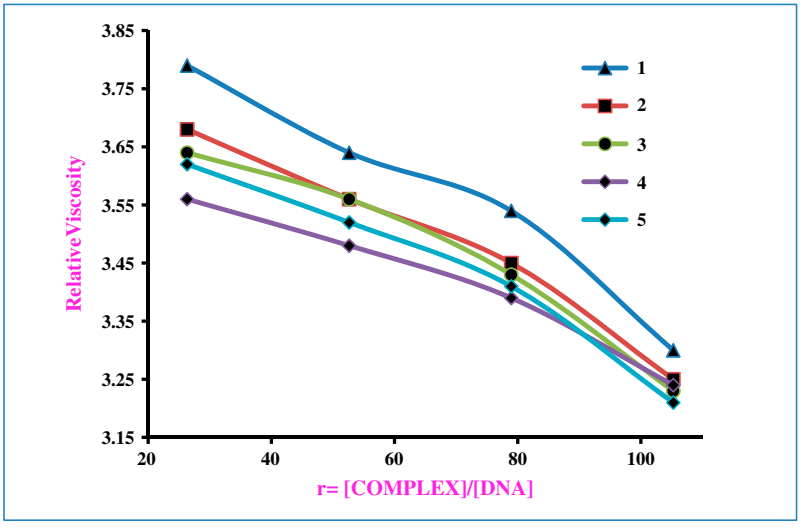

Figure 13. Effect of increasing amount of **1–5** on relative viscosity of SSDNA.

[complex]/[SSDNA] was constructed and it was noted that by increase in concentration of complexes, the viscosity decreases, which indicates that complexes interact with SSDNA through mixed electrostatic and groove binding, as shown in figure 13. This type of interaction of the synthesized complexes with SSDNA was also confirmed by UV–visible spectroscopic technique. Thus, the results of both techniques are in good agreement.

4. Conclusion

Five new O and N-donor zinc(II) complexes have been synthesized in good yield and characterized using elemental analysis, FT-IR, NMR, and X-ray single-crystal analysis. X-ray single-crystal analysis confirmed distorted trigonal bipyramidal geometry for **2** and distorted tetrahedral geometry for **3** and **4**. The structures deduced from FT-IR and NMR data were in agreement with those from single-crystal X-ray analysis. Enzymatic inhibition by the complexes was explored through UV–visible spectroscopy. Those complexes inhibit ALP in a concentration-dependent manner. The complexes were screened for DNA binding through UV–visible spectroscopy and viscometry, both of which revealed a mixed binding mode (hydrogen bonding and groove binding) of interaction of these complexes with DNA. The relatively higher values of the binding constant and negative values of Gibb's free energy indicate the feasibility and spontaneity of the complex–SSDNA interactions. The cyclic voltammetric studies of *para*-nitrophenylacetic acid and its zinc complexes **2** and **3** in aqueous DMSO have shown that all three species possess ligand-centered electro-activity in solution. The effect of coordination to metal on the activity is clearly manifested by the shift in redox potential to less negative potential. The potent DNA binding as well as redox activity of the complexes indicate their potential use in the development of the anti-cancer drugs.

Supplementary material

CCDC numbers 945320–945322 contain the supplementary crystallographic data for **2–4**. These data can be obtained free of charge via http://www.ccdc.cam.ac.uk/conts/retrieving.html, or from the Cambridge Crystallographic Data Center, 12 Union Road, Cambridge CB2 1EZ, UK; Fax: +44 1223 336 033; or E-mail: deposit@ccdc.cam.ac.uk.

Acknowledgement

M. Iqbal is thankful to the Higher Education Commission of Pakistan for providing scholarship.

References

[1] C.N.R. Rao, S. Natarajan, R. Vaidhyanathan. *Angew. Chem. Int. Ed.*, **43**, 1466 (2004).
[2] G. Blay, I. Fernandez, T. Gimenez, J.R. Pedro, R. Ruiz, E. Pardo, F. Lloret, M.C. Munoz. *Chem. Commun.*, 2102 (2001).
[3] Q. Chu, G.X. Liu, Y.Q. Huang, X.F. Wang, W.Y. Sun. *J. Chem. Soc., Dalton Trans.*, 4302 (2007).
[4] P.G. Lassahn, V. Lozan, G.A. Timco, P. Christian, C. Janiak, R.E.P. Winpenny. *J. Catal.*, **222**, 260 (2004).
[5] J.C. Dai, X.T. Wu, Z.Y. Fu, C.P. Cui, S.M. Hu, W.X. Du, L.M. Wu, H.H. Zhang, R.Q. Sun. *Inorg. Chem.*, **41**, 1391 (2002).
[6] M.L. Tong, S. Hu, J. Wang, S. Kitagawa, S.W. Ng. *Cryst. Growth Des.*, **5**, 837 (2005).
[7] M.C. Hong, Y.J. Zhao, W.P. Su, R. Cao, M. Fujita, Z.Y. Zhou, A.S.C. Chan. *Angew. Chem. Int. Ed.*, **39**, 2468 (2000).
[8] O.S. Jung, S.H. Park, K.M. Kim, H.G. Jang. *Inorg. Chem.*, **37**, 5781 (1998).
[9] N. Matsumoto, Y. Motoda, T. Matsuo, T. Nakashima, N. Re, F. Dahan, J.P. Tuchagues. *Inorg. Chem.*, **38**, 1165 (1999).
[10] R.W. Saalfrank, I. Bernt, M.M. Chowdhry, F. Hampel, G.B.M. Vaughan. *Chem. Eur. J.*, **7**, 2765 (2001).
[11] G.B. Deacon, R.J. Phillips. *Coord. Chem. Rev.*, **33**, 227 (1980).
[12] C. Hou, Q. Liu, Y. Lu, T. Okamura, P. Wang, M. Chen, W.Y. Sun. *Microporous Mesoporous Mater.*, **152**, 96 (2012).
[13] B.L. Vallee, D.S. Auld. *Biochemistry*, **29**, 5647 (1990).
[14] E. Kimura, T. Koike. *Adv. Inorg. Chem.*, **44**, 229 (1997).
[15] C.L. Feucht, B.S. Allen, D.K. Chalker. *J. Am. Acad. Dermatol.*, **3**, 483 (1980).
[16] Y.F. Xu, B.Y. Qu, X.H. Qian, Y.G. Li. *Bioorg. Med. Chem. Lett.*, **15**, 1139 (2005).
[17] X. Li, Y. Lin, Q. Wang, Y. Yuan, H. Zhang, X. Qian. *Eur. J. Med. Chem.*, **46**, 1274 (2011).
[18] M.R. Malik, V. Vasylyeva, K. Merz, N. Metzler-Nolte, M. Saleem, S. Ali, A.A. Isab, K.S. Munawar, S. Ahmad. *Inorg. Chim. Acta*, **376**, 207 (2011).
[19] C.L. Tsou. *Adv. Enzymol. Relat. Areas Mol. Biol.*, **61**, 381 (1988).
[20] Z.X. Wang, C.L. Tsou. *J. Theor. Biol.*, **127**, 253 (1987).
[21] J. Fielden, P.T. Gunning, D.L. Long, M. Nutley, A. Ellern, P. Kögerler, L. Cronin. *Polyhedron*, **25**, 3474 (2006).
[22] W.S. Xia, C.H. Huang, D.J. Zhou. *Langmuir*, **13**, 80 (1997).
[23] H. Firouzabadi, M. Adibi, B. Zeynizadeh. *Synth. Commun.*, **28**, 1257 (1998).
[24] P.L. Ng, C.S. Lee, H.L. Kwong, A.S.C. Chan. *Inorg. Chem. Commun.*, **8**, 769 (2005).
[25] Y.C. Shen, Z.J. Li, J.K. Cheng, Y.Y. Qin, Y.G. Yao. *Inorg. Chem. Commun.*, **10**, 888 (2007).
[26] P. Wang, Z. Hong, Z. Xie, S. Tong, O. Wong, C.S. Lee, N. Wong, L. Hung, S. Lee. *Chem. Commun.*, 1664 (2003).
[27] X.X. Xu, Y. Lu, E.B. Wang, Y. Ma, X.L. Bai. *Inorg. Chim. Acta*, **360**, 455 (2007).
[28] G.M. Sheldrick. *Acta Crystallogr., Sect. A: Found. Crystallogr.*, **64**, 112 (2008).
[29] K.S. Munawar, S. Ali, A.N. Khan, S. Shahzadi, S.K. Sharma, K. Qanungo. *ICAIJ*, **7**, 82 (2012).
[30] E. Paleček. *Anal. Biochem.*, **170**, 421 (1988).
[31] J. Marmur. *J. Mol. Biol.*, **3**, 208 (1961).
[32] R. Vijayalakshmi, M. Kanthimathi, V. Subramanian. *Biochem. Biophys. Res. Commun.*, **271**, 731 (2000).
[33] S. Mathur, S. Tabassum. *Cent. Eur. J. Chem.*, **4**, 502 (2006).
[34] V. Zeleňák, Z. Vargová, K. Györyová. *Spectrochim. Acta, Part A*, **66**, 262 (2007).
[35] A. Tavman, I. Boz, A.S. Birteksöz. *Spectrochim. Acta, Part A*, **77**, 199 (2010).

[36] A.A. Alie El-Deen, A.E.E. El-Askalany, R. Halaoui, B.J. Jean-Claude, I.S. Butler, S.I. Mostafa. *J. Mol. Struct.*, **1036**, 161 (2013).
[37] W. Addison, T.N. Rao, J. Reedijk, V.J. Rijn, G.C. Verschoor. *J. Chem. Soc., Dalton Trans.*, 1349 (1984).
[38] S. Caglar, S. Demir, Z. Heren, O. Büyükgüngör. *Polyhedron*, **30**, 1389 (2011).
[39] L.J. Li, X.L. Wang, L. Zhao, K.Z. Shao, H.N. Wang, G. Yuan, Z.M. Su. *Inorg. Chem. Commun.*, **15**, 288 (2012).
[40] R.H. Zhang, W.S. Xia, H. Wang, Z.H. Zhou. *Inorg. Chem. Commun.*, **12**, 583 (2009).
[41] L.B. Ni, R.H. Zhang, Q.X. Liu, W.S. Xia, H. Wang, Z.H. Zhou. *J. Solid State Chem.*, **182**, 2698 (2009).
[42] X.M. Lin, L. Chen, H.C. Fang, Z.Y. Zhou, X.X. Zhou, J.Q. Chen, A.W. Xu, Y.P. Cai. *Inorg. Chim. Acta*, **362**, 2619 (2009).
[43] H. Yin, S.X. Liu. *J. Mol. Struct.*, **918**, 165 (2009).
[44] D. Chen, Y. Wang, Z. Lin, F. Huang. *J. Mol. Struct.*, **966**, 59 (2010).
[45] J. Zhao, X. Shi, G. Li, X. Wang, C. Li, Q. Yang. *Inorg. Chim. Acta*, **383**, 185 (2012).
[46] I. Haque, M. Tariq. *J. Chem. Soc. Pak.*, **33**, 529 (2011).
[47] M. Montazerozohori, M. Sedighipoor. *Spectrochim. Acta, Part A*, **96**, 70 (2012).
[48] S. Shujha, A. Shah, Z. Rehman, N. Muhammad, S. Ali, R. Qureshi, N. Khalid, A. Meetsma. *Eur. J. Med. Chem.*, **45**, 2902 (2011).
[49] Q.S. Li, P. Yang, H. Wang. *J. Inorg. Biochem.*, **64**, 181 (1996).
[50] M.Y. Ni, Y. Wang, H.L. Li. *Pol. J. Chem.*, **71**, 816 (1997).
[51] Y.G. Sun, K.L. Li, Z.H. Xu, T.Y. Lv, S.J. Wang, L.X. You, F. Ding. *J. Coord. Chem.*, **66**, 2455 (2013).
[52] J. Lu, X. Liao, B. Wu, P. Zhao, J. Jiang, Y. Zhang. *J. Coord. Chem.*, **66**, 1574 (2013).
[53] Y.F. Chen, M. Liu, J.W. Mao, H.T. Song, H. Zhou, Z.Q. Pan. *J. Coord. Chem.*, **65**, 3413 (2012).
[54] H. Wu, Y. Bai, J. Yuan, H. Wang, G. Pan, X. Fan, J. Kong. *J. Coord. Chem.*, **65**, 2839 (2012).
[55] M. Jiang, Y. Li, Z. Wu, Z. Liu, C. Yan. *J. Inorg. Biochem.*, **103**, 833 (2009).